Comparing the Degree of Land–Atmosphere Interaction in Four Atmospheric General Circulation Models

RANDAL D. KOSTER,* PAUL A. DIRMEYER,+ ANDREA N. HAHMANN,# RUBEN IJPELAAR,@ LORI TYAHLA,& PETER COX,** AND MAX J. SUAREZ++

*Hydrological Sciences Branch, Laboratory for Hydrospheric Processes, NASA Goddard Space Flight Center, Greenbelt, Maryland
+Center for Ocean–Land–Atmosphere Studies, Calverton, Maryland
#Institute of Atmospheric Physics, The University of Arizona, Tucson, Arizona
@Wageningen University, Wageningen, Netherlands
&Global Science and Technology, Inc., Lanham, Maryland
**Hadley Centre for Climate Prediction and Research, Met Office, Berkshire, United Kingdom
++Climate and Radiation Branch, Laboratory for Atmospheres, NASA Goddard Space Flight Center, Greenbelt, Maryland

(Manuscript received 16 May 2001, in final form 12 December 2001)

ABSTRACT

The strength of the coupling between the land and the atmosphere, which controls, for example, the degree to which precipitation-induced soil moisture anomalies affect the overlying atmosphere and thereby the subsequent generation of precipitation, has been examined and quantified with many atmospheric general circulation models (AGCMs). Generally missing from such studies, however, is an indication of the extent to which the simulated coupling strength is model dependent. Four modeling groups have recently performed a highly controlled numerical experiment that allows an objective intermodel comparison of land–atmosphere coupling strength, focusing on short (weekly down to subhourly) timescales. The experiment essentially consists of an ensemble of 1-month simulations in which each member simulation artificially maintains the same (model specific) time series of surface prognostic variables. Differences in atmospheric behavior between the ensemble members then indicate the degree to which the state of the land surface controls atmospheric processes in that model. A comparison of the four sets of experimental results shows that coupling strength does indeed vary significantly among the AGCMs.

1. Introduction

The impact of precipitation anomalies on soil moisture anomalies is self-evident—heavy rains induce wet soil, whereas extended dry periods induce dry soil. Less obvious is the impact of soil moisture anomalies on the precipitation itself. Conceivably, a wetter soil can produce higher evaporation, which in turn can induce additional precipitation through both local recycling and modifications in the large-scale circulation. This land–atmosphere feedback, if strong, is of great interest. It may allow, for example, the translation of soil moisture anomalies into short-term and seasonal predictions of precipitation.

The feedback between soil moisture and precipitation is but one manifestation of the coupling between the land surface and the atmosphere. This coupling, by which variations in land surface properties induce variations in the atmosphere, indeed occurs over a wide range of temporal scales. At shorter (e.g., hourly) timescales, variations in surface temperature can induce variations in evaporation and sensible heat flux that can in turn strongly affect the evolution of the atmospheric boundary layer. Rainwater intercepted on the vegetation canopy evaporates very quickly and thus has its own impact on short timescales. At very long timescales (annual and decadal), variations in climate can induce variations in vegetation structure, which in turn can feed back on the climate itself.

Atmospheric general circulation models (AGCMs) are popular tools for examining the land–atmosphere coupling problem, largely because they include parameterizations for many of the physical processes involved and because these parameterizations can be manipulated easily in controlled experiments. The list of published feedback studies is extensive (e.g., Shukla and Mintz 1982; Henderson-Sellers and Gornitz 1984; Delworth and Manabe 1989; Oglesby and Erickson 1989; Dirmeyer 1994; Lau and Bua 1998; Schar et al. 1999; to name only a few). Necessarily missing from single-AGCM experiments, however, is an analysis of the degree to which the experimental results are model-dependent. Models can certainly differ in the strength of the coupling; differences in land-surface parameteriza-

Corresponding author address: Randal D. Koster, Hydrological Sciences Branch, NASA GSFC Code 974, Greenbelt, MD 20771.
E-mail: randal.koster@gsfc.nasa.gov

tions, for example, can lead to differences in the response of evaporation to precipitation anomalies, and differences in boundary layer and convection parameterizations can lead to differences in the atmosphere's response to anomalies of surface evaporation and sensible heat flux. Clearly, in any land–atmosphere AGCM study, an evaluation of simulated coupling strength against observations is desirable.

Unfortunately, while a few indirect approaches have been employed at the regional scale (e.g., Findell and Eltahir 1997), the direct quantification of real-world coupling strength at the global scale from available observations is extremely difficult, if not impossible. The validation of simulated coupling strength is indeed beyond the scope of this paper. This paper instead focuses on a lesser, but still very important, aspect of the problem: the extent to which simulated coupling strength varies between different AGCMs. This variation is a measure of the degree to which various land–atmosphere model results are model-dependent. In a sense, it measures the uncertainty inherent in our understanding of the coupling and our ability to model it.

The problem of intermodel variation in coupling strength—particularly at the shorter timescales, weekly down to hourly—is addressed here by having several AGCMs perform the same, highly controlled numerical experiment. Four models participated in the intercomparison: the National Aeronautic and Space Administration (NASA) Seasonal-to-Interannual Prediction Project (NSIPP) AGCM, the Center for Ocean–Land–Atmosphere Studies (COLA) AGCM, the National Center for Atmospheric Research (NCAR) Community Climate Model version 3 (CCM3) coupled to the Biosphere–Atmosphere Transfer Scheme (BATS), and the Hadley Centre/Met Office AGCM (HadAM3). The experiment is described in section 2, and the results of the intercomparison are presented in section 3. Section 4 offers some interpretation of the results.

2. Experiment design

The design of the experiment is illustrated in Fig. 1. The experiment has two parts. In the first part, the AGCM, fully coupled to its own land surface model (LSM) but forced by prescribed sea surface temperatures (SSTs), is run over a selected month. At each time step in this simulation (hereinafter labeled simulation W, for ''write''), the values of all land surface prognostic variables at every grid cell are recorded into a special data file. The recorded prognostic variables include soil moisture contents at all vertical levels, temperatures at all vertical levels, canopy interception reservoir content, and various variables characterizing snow, if snow is present. The 1-month experiment is then repeated 15 more times, using 15 different sets of atmospheric and land surface initial conditions, to obtain an ensemble of 16 1-month simulations (simulations W1–W16). The prognostic variables, however, are only recorded during simulation W1.

The second part of the experiment consists of another 16-member ensemble of 1-month simulations, using solar forcing for the same month as before and using the same prescribed SSTs. Again, the ensemble members use different atmospheric initial conditions. At every time step of every simulation, the updated values of all land surface prognostic variables are discarded and then replaced by the corresponding values for that time step from the data file written in simulation W1. Thus, in this ensemble, all member simulations (simulations R1–R16, where R denotes ''read'') are forced to maintain precisely the same time series of (geographically varying) land surface states.

We focus mainly on precipitation in this study. The idea is simple: we examine the degree to which the time series of precipitation rates in simulations R1–R16 are similar. If they are similar, even after ''subtracting out'' the effects of SSTs and other intramonthly signals through an analysis of simulations W1–W16, then we can say that the evolution of the atmosphere is indeed largely governed by land surface conditions. The degree to which the intraensemble similarity differs between AGCMs provides one measure of how land–atmosphere feedback strength varies between them. The time steps used in the simulations, of course, capture diurnal variations in surface temperature and canopy interception reservoir content; thus, this experiment focuses on the hourly to weekly timescales of land–atmosphere coupling. (A supplemental experiment, described in section 4c, shows that the hourly and weekly timescales in fact have different impacts on precipitation.)

The setup of the experiment did differ slightly between the four participating AGCMs. For example, for various reasons, each AGCM used its own set of prescribed SSTs, though each set was derived from datasets used in various phases of the Atmospheric Model Intercomparison Project (AMIP; Gates 1992). The various differences are described in detail in the appendix. As shown in section 4b, the differences should have very little impact on the basic outcome of the experiment. (A possible exception, however, involves the setup of the HadAM3 experiment, which did not prescribe the canopy interception reservoir content during the R ensemble. Implications of this are discussed in section 4a.)

3. Results

To quantify the degree of ''similarity'' in the time series of precipitation amongst the members of an ensemble, we employ an approach used by Koster et al. (2000). First, we choose an aggregation period. In the analysis below, we look at 3-day totals of precipitation, P; each July simulation thus provides, at each grid cell, a times series of 10 3-day totals. We then compute an ensemble average time series $\hat{P}$ for the grid cell. For each time period n, we compute

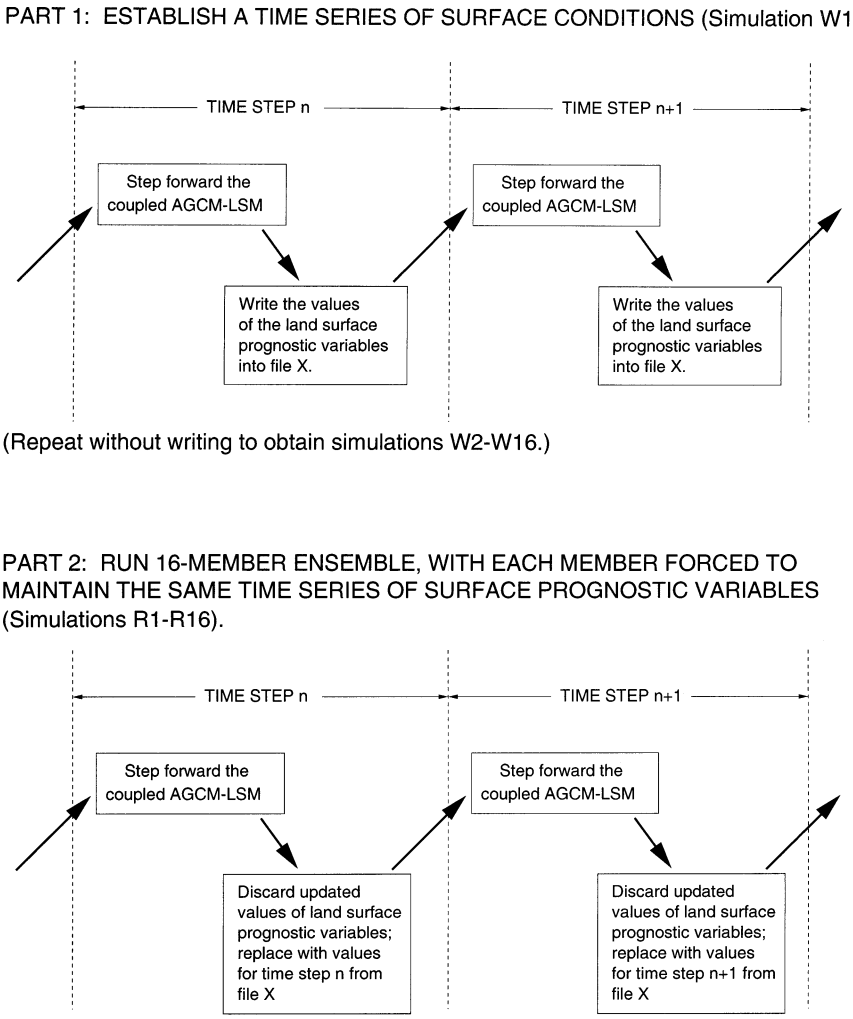

FIG. 1. Basic design of the experiment, as performed by all participating models.

$$\hat{P}_n = \frac{1}{16}\sum_{i=1}^{16} P_{ni}, \tag{1}$$

where i loops over the 16 ensemble members. Next, we compute the variance, σ_P^2, of P across all ensemble members and time periods (i.e., across 160 values) and the variance, $\sigma_{\hat{P}}^2$, of $\hat{P}$ across all time periods (i.e., across 10 values). This allows us to compute Ω_P at the grid cell, a measure of time series similarity:

$$\Omega_P = \frac{16\sigma_{\hat{P}}^2 - \sigma_P^2}{15\sigma_P^2}. \tag{2}$$

Note that if each ensemble member produces exactly the same time series of P, then $\sigma_{\hat{P}}^2$ will equal σ_P^2, and Ω_P will equal 1. If, however, the time series are completely uncorrelated, then $\sigma_{\hat{P}}^2$ will be approximately $\sigma_P^2/16$, and Ω_P will be about 0. Thus, Ω_P varies from 0 to 1, with values closer to 1 indicating a greater degree of precipitation similarity.

Essentially, Ω_P measures the ratio of the signal variance to the total variance. (A similar diagnostic was suggested by Rowell et al. (1995).] Figure 2 illustrates the nature of Ω_P graphically. The top plot in the figure shows the time series of precipitation at a specific grid cell for each of the 16 simulations in the NSIPP R ensemble. Note that the precipitation is low for the month until day 20, when it becomes large for each simulation. The obvious coherence between the different time series is reflected in the high Ω_P value (0.85) at this grid cell. In the bottom plot, which shows the 16 time series at a different grid cell, the coherence is absent—the precipitation generated in one simulation is essentially independent of that in any other simulation. Precipitation at this cell is thus controlled by chaotic atmospheric dynamics rather than by SST or land conditions. For this grid cell Ω_P is very low (0.07).

To relate Ω_P to land control, we must properly account for seasonal variations in SSTs and anything else outside of the land surface that can induce intramonthly trends in precipitation. We do this simply by calculating Ω_P

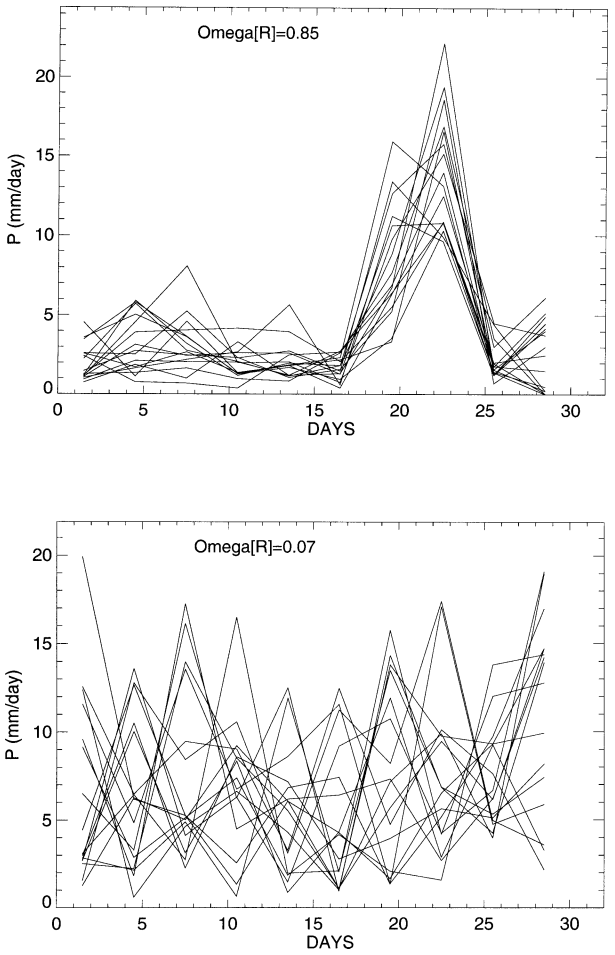

FIG. 2. Superposed time series of precipitation (mm day^{-1}), as produced by the NSIPP model's R ensemble. (top) Grid cell for which Ω_P is high. (bottom) Grid cell for which Ω_P is low.

separately for the R and W ensembles: $\Omega_P(R)$ represents the similarity in precipitation induced by all factors, including the specified set of land states, and $\Omega_P(W)$ represents the similarity induced by everything but the specified land states. The difference $\Omega_P(R) - \Omega_P(W)$ thus gives a first-order indication of the land's impact on the evolution of the atmosphere.

Global maps of $\Omega_P(R) - \Omega_P(W)$ are provided in Fig. 3 for all four AGCMs. The salient result is a wide disparity in the diagnostic between the models. The impact of land conditions on atmospheric processes is clearly largest for the NSIPP model. The COLA and CCM3/BATS models have similar $\Omega_P(R) - \Omega_P(W)$ distributions, with values of 0.2 or less almost everywhere, and the HadAM3 model has what appears to be an even weaker land–atmosphere connection.

Because the choice of a 3-day averaging period was somewhat arbitrary, other averaging periods were examined as well. The relative behavior of the models is similar when the precipitation is averaged over 1- and 6-day periods (not shown). In general, however, $\Omega_P(R) - \Omega_P(W)$ for a given model increases as the precipitation aggregation period increases.

4. Discussion

a. Coherence of surface fluxes

One potential explanation for low values of $\Omega_P(R) - \Omega_P(W)$ in Fig. 3 involves the response of the surface turbulent fluxes to the imposed surface states. Because of variations in the atmospheric forcing, the time series of evaporation or sensible heat flux among the members of an ensemble may not look the same, even given identical time series of soil moisture and temperature. If the time series of turbulent fluxes were not the same, and if the effect of the land surface on precipitation were mostly through these fluxes, then the derived values of $\Omega_P(R) - \Omega_P(W)$ would necessarily be low.

A warning is in order here: the response of precipitation to land surface conditions may be more complex than this. For example, the temperature and humidity conditions in the atmospheric boundary layer, which help determine precipitation, may be strongly guided by surface temperature and moisture states. Although the surface fluxes are responsible for communicating these surface states to the boundary layer, the state of the boundary layer may nevertheless correlate better with the surface states themselves than with the *time-integrated* surface fluxes examined in this section.

With this caveat, we analyze the time series of evaporation rates produced by the AGCMs by defining, in direct analogy to Ω_P, the diagnostic Ω_E:

$$\Omega_E = \frac{16\sigma_{\hat{E}}^2 - \sigma_E^2}{15\sigma_E^2}, \tag{3}$$

where σ_E^2 is the variance of evaporation across all ensemble members and $\sigma_{\hat{E}}^2$ is the variance of evaporation in the ensemble mean time series. Thus, Ω_E measures the degree of similarity among the time series of evaporation rates (and loosely, via energy balance considerations, among the time series of sensible heat fluxes) produced by the different members of an ensemble. As with Ω_P, a value of 1 implies that all 16 time series are identical, whereas a value of 0 implies that the 16 time series are completely uncorrelated.

Figure 4 shows the global distribution of $\Omega_E(R) - \Omega_E(W)$ for each of the AGCMs. In each case, $\Omega_E(R) - \Omega_E(W)$ is high over much of the globe. Thus, in many regions, specifying surface moisture and temperature states in this experiment is roughly equivalent to specifying time series of the surface turbulent fluxes. If $\Omega_P(R) - \Omega_P(W)$ is correspondingly low in these regions, as it is, in particular, for the COLA, CCM3/BATS, and HadAM3 AGCMs, then we can conclude that the modeled atmosphere in these regions does not respond strongly to the local surface fluxes. That is, a low $\Omega_P(R) - \Omega_P(W)$ value in the presence of a high $\Omega_E(R) - \Omega_E(W)$ value is probably best explained by the model's

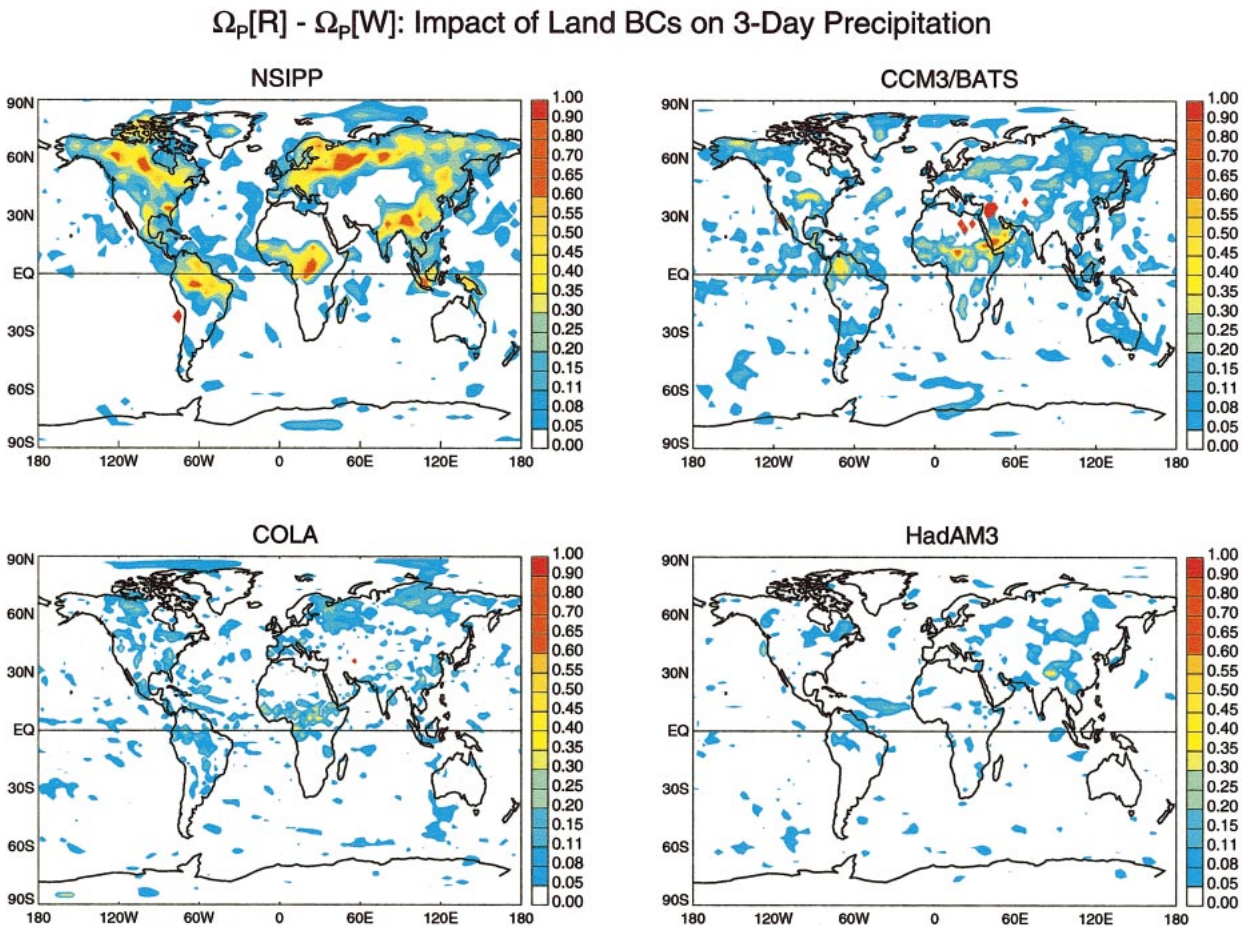

FIG. 3. Global fields of $\Omega_P(R) - \Omega_P(W)$, as generated by each of the participating AGCMs.

atmospheric formulations, presumably those of boundary layer processes and moist convection, though it might also (or instead) result from a low $\Omega_E(R) - \Omega_E(W)$ value in a critical remote region.

The fact that $\Omega_E(R) - \Omega_E(W)$ is large in many regions for HadAM3 is reassuring, since the interception reservoir content was not prescribed in this particular model's R ensemble. The large $\Omega_E(R) - \Omega_E(W)$ values for HadAM3 suggest that the correspondingly low $\Omega_P(R) - \Omega_P(W)$ values in Fig. 3 do not result solely from this aspect of this model's experimental design. Nevertheless, HadAM3 does show low values of $\Omega_E(R) - \Omega_E(W)$ over, for example, much of North America, tropical Africa, India, and Southeast Asia. These low values may be due in part to freely evolving canopy interception. They may also be due, however, to the fact that evaporation in the HadAM3 model is rarely moisture-limited (Gedney et al. 2000), for when a region is energy-limited rather than moisture-limited, the aforementioned impact of atmospheric variability on the surface fluxes is strong.

Indeed, for any model, we expect that an area with evaporation that is strongly energy-limited should have a lower value of $\Omega_E(R) - \Omega_E(W)$. Such behavior is particularly apparent in the CCM3/BATS and COLA models, as demonstrated in Fig. 5. For these two models, the figure shows the average relationship (the solid line) between $\Omega_E(R) - \Omega_E(W)$ and the ratio of evaporation to precipitation, *E*/*P*. (A simple binning procedure was used to construct each curve.) Here *E*/*P* is used as a simple ''dryness index,'' with low values implying that evaporation is strongly energy-limited. On average, $\Omega_E(R) - \Omega_E(W)$ is significantly reduced for small values of *E*/*P*, implying that energy-versus-water limitations explain some of the spatial patterns seen in Fig. 4. As a consequence, $\Omega_P(R) - \Omega_P(W)$ (shown as the dotted line in Fig. 5) is also reduced for small values of *E*/*P*. The relationships between $\Omega_E(R) - \Omega_E(W)$ and *E*/*P* in the NSIPP and HadAM3 models (not shown) are not nearly so clear, perhaps (for HadAM3) due to the influence of canopy interception, or perhaps because neither of these two models produce many *E*/*P* values below 0.2.

b. Potential limitations of experiment

The results in Fig. 3 may be limited by the idealized nature of the experiment and by various logistical dif-

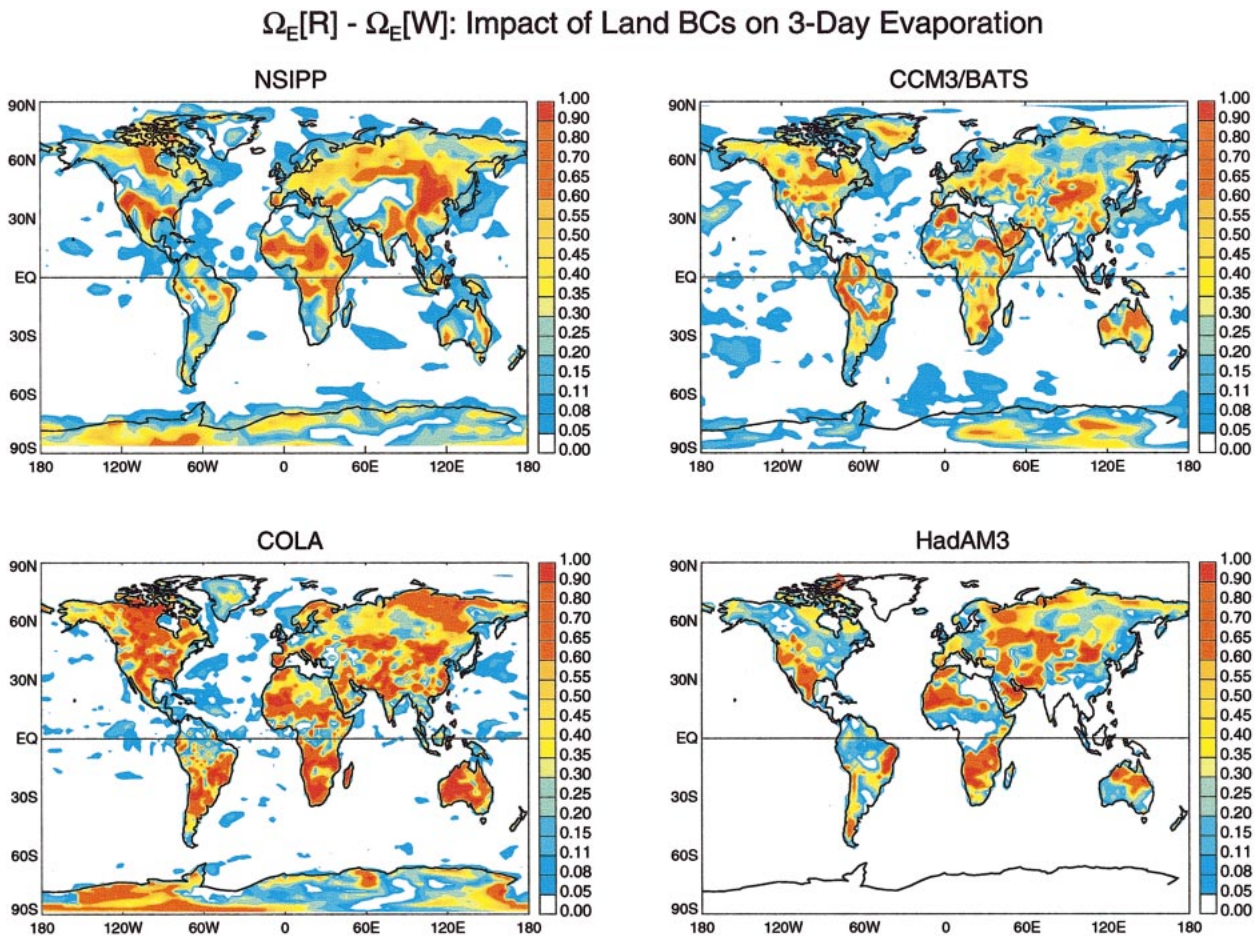

FIG. 4. Global fields of $\Omega_E(R) - \Omega_E(W)$, as generated by each of the participating AGCMs. Note that oceanic evaporation rates for HadAM3 were zeroed prior to processing.

ficulties associated with its coordination across a number of modeling groups. In this section we evaluate several of these potential limitations. To save space, we focus on the spatially averaged value of $\Omega_P(R) - \Omega_P(W)$ over ice-free land, $[\Omega_P(R) - \Omega_P(W)]$, rather than on global maps of the diagnostic.

1) DIFFERENCES IN SST FIELDS

For various reasons, the four modeling groups used SST fields from different Julys: 1988 SSTs were used by NSIPP, 1983 SSTs by CCM3/BATS, 1986 SSTs by COLA, and 1981 SSTs by HadAM3. If certain SST conditions are more conducive than others to promoting land–atmosphere interaction, then the intermodel differences in prescribed SSTs may have compromised the comparisons in Figs. 3 and 4.

This issue is addressed with supplementary simulations performed with the NSIPP model. The NSIPP W and R ensembles were both repeated three times: once with SSTs from 1981, once with SSTs from 1983, and once with SSTs from 1986. The resulting values of $[\Omega_P(R) - \Omega_P(W)]$ for each year are shown in the top panel of Fig. 6. The salient feature of the plot is the relatively small sensitivity of $[\Omega_P(R) - \Omega_P(W)]$ to the prescribed SSTs. [The global patterns of $\Omega_P(R) - \Omega_P(W)$, not shown, are similar between the years.] At least for the NSIPP model, the year chosen for the experiment appears secondary. The top panel of Fig. 6 allows a comparison of the NSIPP model with each other model under the same prescribed SSTs; in each case, the earlier conclusion is confirmed—land–atmosphere interaction appears stronger in the NSIPP model.

2) DIFFERENT CHOICES FOR SPECIFIED SURFACE CONDITIONS

Each modeling group chose a single member of its W ensemble to specify the time series of surface states for its R ensemble. This simulation, labeled W1, was effectively chosen at random from the 16 members of the W ensemble. This suggests an obvious question: if another member of a given model's W ensemble was labeled W1 instead, that is, if another set of prescribed

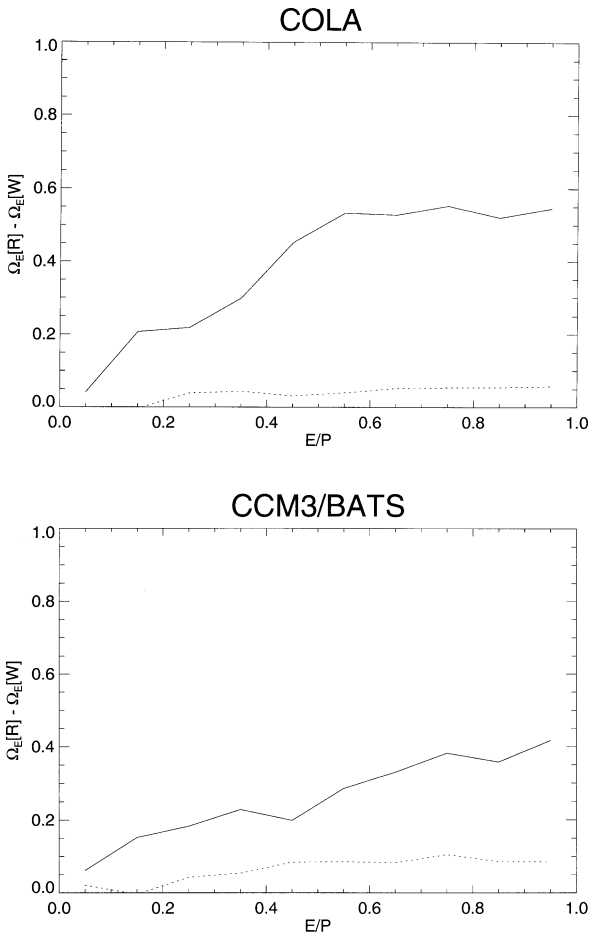

FIG. 5. Average relationship between E/P and $\Omega_E(R) - \Omega_E(W)$ (solid line) and between E/P and $\Omega_P(R) - \Omega_P(W)$ (dotted line) for the COLA and CCM3/BATS models. A simple binning procedure was used to construct the curves, with bins having an E/P range of 0.1.

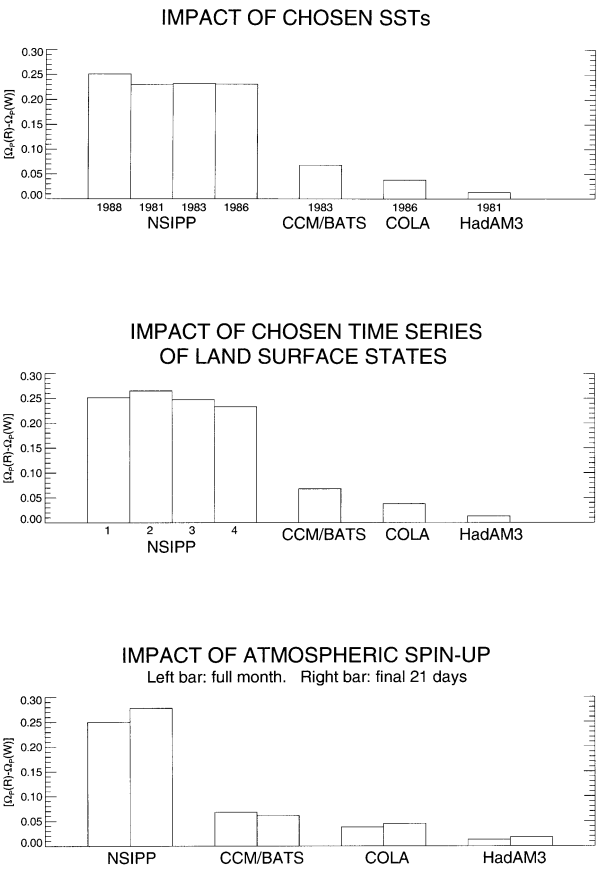

FIG. 6. Examination of potential limitations to the numerical experiment, focusing on the average value of $\Omega_P(R) - \Omega_P(W)$ over land, $[\Omega_P(R) - \Omega_P(W)]$. (top) Impact of SSTs used. For the NSIPP model, each bar represents the $[\Omega_P(R) - \Omega_P(W)]$ value obtained under a different set of SSTs. The values obtained for the other models are shown for comparison. (middle) Impact of choice of the time series of land surface states used in the R ensemble. For the NSIPP model, each bar corresponds to the $[\Omega_P(R) - \Omega_P(W)]$ obtained when a different member of the W ensemble is used to establish the states. The values obtained for the other models are shown for comparison. (bottom) Impact of atmospheric ''spinup'' effects on $[\Omega_P(R) - \Omega_P(W)]$. The height of the left bar associated with each model is computed from all of the data for the month, and that of the right bar is computed from the final 21 days of data.

surface states were used in the model's R ensemble, would the computed value of $[\Omega_P(R) - \Omega_P(W)]$ change? In other words, to what extent must we consider a model's own inherent variability when choosing the time series of imposed surface states?

This question is examined with some additional NSIPP model simulations. Three additional 16-member R ensembles were constructed with the NSIPP model, using three different members of the NSIPP W ensemble to specify the surface states. The resulting variation in $[\Omega_P(R) - \Omega_P(W)]$ is shown in the middle panel of Fig. 6. The variation between the four NSIPP ensembles is clearly much smaller than the variation between the different models, suggesting that the results in Fig. 3 are not affected, at least to first order, by the choice of the W ensemble member used to specify the surface states.

3) INITIAL ATMOSPHERIC CONDITIONS

The 16-member R ensemble is constructed by initializing the atmospheric conditions with 16 different sets of states, taken directly from the corresponding members of the W ensemble. Thus, in all but one member of the R ensemble, the atmospheric initial conditions are not in equilibrium with the prescribed time series of land surface states. The associated initial ''shock'' to the system could affect atmospheric behavior in the first several days of each simulation. It could thus affect the computed values of $\Omega_P(R) - \Omega_P(W)$.

To investigate this, we recomputed $[\Omega_P(R) - \Omega_P(W)]$ after dismissing the first 10 days of each simulation; that is, we computed $[\Omega_P(R) - \Omega_P(W)]$ from the final seven 3-day periods in July. The results are shown in the bottom plot of Fig. 6. Eliminating the first 10 days does not strongly affect the computed intermodel differences in $[\Omega_P(R) - \Omega_P(W)]$. This suggests that at-

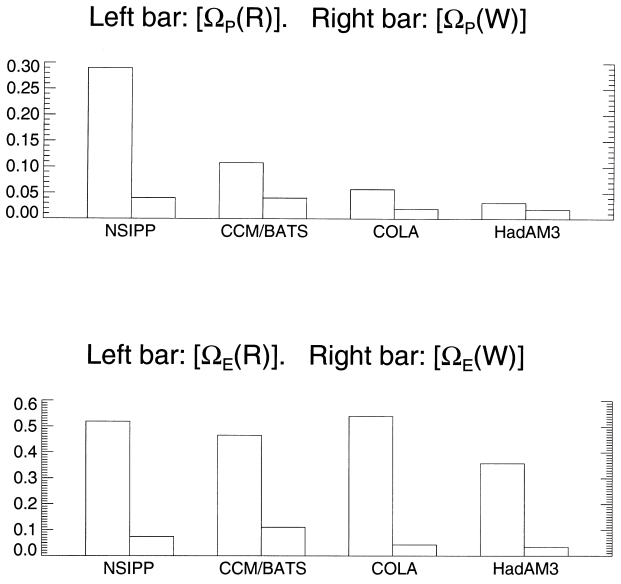

FIG. 7. (top) Average values of $\Omega_P(R)$ and $\Omega_P(W)$ over land for each model. (bottom) Same, but for $\Omega_E(R)$ and $\Omega_E(W)$.

mospheric spinup problems do not strongly limit the experimental design.

4) POTENTIAL FOR HIGH Ω VALUES IN THE W ENSEMBLE

Figure 3 shows the global distribution of $\Omega_P(R) - \Omega_P(W)$. If $\Omega_P(W)$ is already close to 1, as due perhaps to the influence of neighboring SSTs, then the difference $\Omega_P(R) - \Omega_P(W)$ would necessarily be small. A look at the individual $\Omega_P(W)$ and $\Omega_P(R)$ values, with an eye toward whether high $\Omega_P(W)$ values could cloud the model intercomparison, is thus instructive.

Global maps of $\Omega_P(W)$ (not shown) indicate that the diagnostic is never very large over continents. A few moderate values are seen here and there over tropical and subtropical continents; as an extreme example, $\Omega_P(W)$ over part of India exceeds 0.35 for CCM3/BATS. The top panel of Fig. 7 shows the continental averages $[\Omega_P(R)]$ and $[\Omega_P(W)]$ for each model. Clearly, $[\Omega_P(W)]$ is small relative to $[\Omega_P(R)]$, except for HadAM3, for which both are small. Similarly, as shown in the bottom panel of Fig. 7, $[\Omega_E(W)]$ is small relative to $[\Omega_E(R)]$. Thus, taking the difference between the W and R ensembles does not mask any high precipitation or evaporation coherence.

c. ''Fast'' versus ''slow'' reservoirs

One curious aspect of Fig. 3 is the geographical structure of the NSIPP model's $\Omega_P(R) - \Omega_P(W)$ distribution, which differs somewhat from the corresponding seasonal distribution derived by Koster et al. (2000) with the same AGCM. Koster et al. (2000) place the largest Ω_P differences in the transition zones between arid and humid regions, whereas Fig. 3 places them in somewhat different areas, farther to the north, for example, in North America and Asia. The difference results from the different designs of the experiments. In Koster et al. (2000), only the soil moisture—the ''slow'' component of the land system—is effectively prescribed. In the present analysis, the fast components (the interception reservoir, the surface temperature, etc.) are also prescribed, and these fast components have their own unique impact on precipitation.

To isolate this unique impact, the R ensemble is repeated two more times with the NSIPP model. In the first rerun, only the two lower soil moisture layers (which encompass the root zone and a lower recharge volume) are updated at each time step from the file written by the W1 simulation; all other land variables are free to evolve with the atmosphere. [Note that this approach is reminiscent of the ''relaxation'' approach used in the literature (e.g., Douville et al. 2001) to update slow components toward desired values, though the relaxation time used here is zero.] In the second rerun, all three soil moistures, the interception reservoir, and the snow cover are updated from the W1 file at each time step, while the temperatures are free to evolve with the atmosphere.

Values of $\Omega_P(R) - \Omega_P(W)$ for the second rerun are shown in the top panel of Fig. 8. The patterns for the first rerun, not shown, are quite similar. When the temperatures are not updated, the strength of $\Omega_P(R) - \Omega_P(W)$ for the NSIPP model is strongly diminished relative to that shown in Fig. 3. Furthermore, the spatial patterns shown in Fig. 8 (though not the magnitudes, due to the difference in averaging time) are much more consistent with those identified by Koster et al. (2000). A clue to the reduction in $\Omega_P(R) - \Omega_P(W)$ is provided in the lower panel of Fig. 8, which shows the global map of $\Omega_E(R) - \Omega_E(W)$ for the second rerun. When the surface temperatures are free to evolve with the atmosphere, the evaporation signal in the northern reaches of North America and Asia is no longer coherent between the simulations, suggesting that the precipitation signal there cannot be coherent either. We warn again that this type of argument may oversimplify the AGCM's behavior; as discussed in section 4a, the nature of the boundary layer in the NSIPP model (or any model) may be guided more directly by variations in temperature than by variations in evaporation. Still, the different impacts of the ''fast'' and ''slow'' components of the land system on precipitation are, at least for the NSIPP model, made clear in the comparison of Figs. 3 and 8.

Whether the NSIPP model's $\Omega_P(R) - \Omega_P(W)$ values would still exceed those of the other three models in an experiment that focused strictly on the slower components of the feedback cannot be determined without additional, corresponding runs made with the other models. Note also that such a ''slow component'' analysis would have more direct relevance to predictability studies, since these are the components that may be pre-

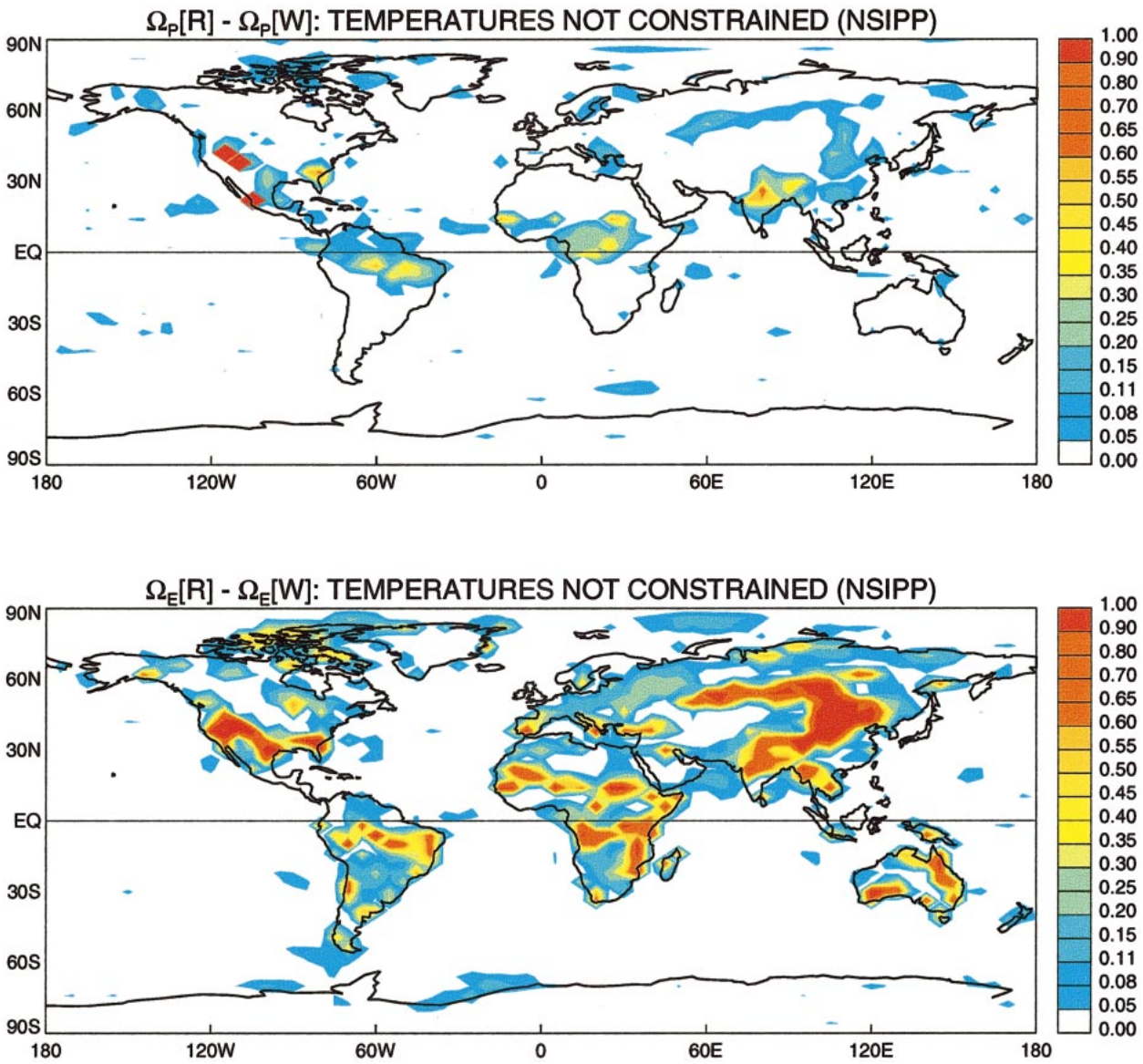

FIG. 8. (top) Global field of $\Omega_P(R) - \Omega_P(W)$, as generated by a supplemental NSIPP experiment in which surface temperature and deep soil temperature are not prescribed from the file written by simulation W1. (bottom) Same, but for $\Omega_E(R) - \Omega_E(W)$.

dictable (and thus effectively ''specified'') on seasonal timescales due to their inherent memory. This underscores the idealized nature of the present intercomparison study. The intercomparison in Fig. 3 does not address the long-term predictability of precipitation in the participating models. It simply allows a highly controlled comparison of the models' coupling behavior—a comparison of the degree to which the generation of precipitation is guided by the full land surface state (including the short-term, hourly variations) rather than by chaotic atmospheric dynamics or external forcings (SSTs). Clearly the models disagree about the strength of this land–atmosphere coupling. Such uncertainty is often not acknowledged in land–atmosphere feedback studies.

We must emphasize again that the proper level of land–atmosphere coupling strength—the proper range of $\Omega_P(R) - \Omega_P(W)$ [or even $\Omega_E(R) - \Omega_E(W)$]—is simply not known. This analysis makes no attempt to state which model's coupling behavior is the most realistic. For a proper evaluation, long-term observational studies of boundary layer behavior are required. Furthermore, the low $\Omega_P(R) - \Omega_P(W)$ values in Fig. 3 for the COLA, CCM3/BATS, and HadAM3 models do not imply that these models have a low potential for predictability. The COLA group recently performed a series of experiments similar to those of Koster et al. (2000). An analysis of these experiments shows that the coupling behavior of the COLA model on seasonal timescales is similar to that of the NSIPP model—in effect, $\Omega_P(R) - \Omega_P(W)$

for both models is high over a significant fraction of the earth. Apparently the noise behind the COLA model's low $\Omega_P(R) - \Omega_P(W)$ values in Fig. 3 is smoothed out at much longer timescales.

5. Summary

A highly idealized, simple, and inexpensive AGCM experiment has been devised that illustrates some key aspects of simulated land–atmosphere coupling behavior. Four AGCM groups have performed the experiment for the present study, and a comparison of their results shows that the apparent strength of land–atmosphere coupling on short (hourly to weekly) timescales does vary significantly between the models. A strict evaluation against observations is not provided, since the strength of coupling in the real world is difficult to measure. Nevertheless, the intermodel differences are important in themselves, since they illustrate the uncertainty with which we understand the various processes (particularly atmospheric boundary layer and convection processes) that control the coupling.

Further studies of coupling strength are needed. A modified set of experiments, designed to avoid the limitations outlined in section 4b and to address, in addition, the slow components of the coupling (see section 4c), could in principle be performed by an even greater number of AGCM groups. This would serve to establish more completely the broad range of coupling behavior inherent in AGCMs today. Furthermore, field observation campaigns that begin to address the strength of coupling in the real world need to be designed. Advancement in our understanding of the coupling is critical, given the central role it plays in many published and ongoing numerical studies of climate variability and predictability.

Acknowledgments. The NSIPP model runs were funded by the Earth Science Enterprise of NASA Headquarters through the EOS-Interdisciplinary Science Program and the NASA Seasonal-to-Interannual Prediction Project (NSIPP), with computational resources provided by the NASA Center for Computational Sciences. The UKMET effort was supported by the U.K. DEFRA Climate Prediction Programme (Contract PECD 7/12/37). The COLA model runs were funded by NSF Grant ATM 9814265, NOAA Grant NA96GP0056, and NASA Grant NAG5-8202. The CCM3/BATS runs were supported by DOE CCPP Grant PEFG-0398-ER-6206 and NOAA PACS Grant NA06GP0360.

APPENDIX

Details of Experimental Designs

a. NSIPP

The NSIPP atmospheric AGCM, a component of the NSIPP seasonal forecasting system, is a multilevel primitive equation model that includes penetrative convection with the Relaxed Arakawa–Schubert scheme (Moorthi and Suarez 1992) and Richardson number–dependent fluxes in the surface layer (Louis et al. 1982). Atmospheric dynamics are coded as a dynamical core (Suarez and Takacs 1995), with fourth-order advection of vorticity and all scalars. The model's reproduction of observed precipitation means and variability is discussed by Koster et al. (2000).

The NSIPP AGCM is coupled to the Mosaic LSM (Koster and Suarez 1992, 1996), a soil–vegetation–atmosphere transfer (SVAT) scheme that includes explicit vegetation control over the surface energy balance. The scheme accounts for subgrid variability in surface characteristics by partitioning heterogenous grid squares into relatively homogeneous subregions (''tiles'' of the mosaic) and then computing separate energy and water balances over each tile. For the R ensemble, values of four prognostic moisture variables at each tile are continually read in: one for canopy interception reservoir storage and one for each of three soil layers (a thin layer near the surface, a middle layer that encompasses the remainder of the root zone, and a lower ''recharge'' layer for long-term storage). A surface temperature and a deep soil temperature are also read in, as is a snow mass, if snow is present. Last, a within-canopy humidity is read in for the R ensemble, but this particular specification has little, if any, impact; the value read-in is merely an ''initial guess'' to the actual value used by the model, a value that is corrected at each time step so that the flux of moisture into the canopy air equals the flux out of the canopy air. Thus, despite its apparent specification, the within-canopy humidity does evolve with the atmosphere.

For the present analysis, the NSIPP AGCM was run at a resolution of 4° lat × 5° lon and used prescribed July SSTs from 1988. Sixteen preexisting multidecade AMIP simulations (i.e., simulations using SSTs prescribed from observations), run in parallel, provided the 16 sets of 1 July 1988 atmospheric and land surface states used to initialize the W ensemble. The same 16 sets of atmospheric and land conditions were used to initialize the R ensemble. (Of course, given the design of the experiment, the initialization of the land states for the R ensemble is irrelevant.)

b. CCM3/BATS

The Community Climate Model version 3 (CCM3) is a spectral model that is the atmospheric component of the NCAR Climate System Model (CSM-1; Boville and Gent 1998). The version of CCM3 used here is CCM3.2, run at T42 resolution, with 18 vertical levels and with a model top at 2.9 hPa. This model includes the parameterization of moist convection developed by Zhang and McFarlane (1995) that operates in conjunction with the shallow convection scheme of Hack (1994). Cloud frac-

tions and optical properties are computed diagnostically from large-scale variables and convective mass fluxes. An updated version of the nonlocal boundary layer parameterization of Holtslag and Boville (1993) is used to determine boundary layer turbulent fluxes. Further details on the model can be found in Kielh et al. (1998), which also includes an evaluation of the model performance.

In the model used here, the standard CCM3 land surface model (LSM; Bonan 1998) has been replaced with the Biosphere–Atmosphere Transfer Scheme (BATS) described in Dickinson et al. (1993). An evaluation of the climate simulated by CCM3/BATS as compared with the one simulated by the standard model can be found in Hahmann and Dickinson (2001). BATS uses the ''big leaf'' approach to describe the processes occurring at the interface between the atmosphere and the land surface. One vegetation layer and three soil layers, accounting for seven prognostic variables (canopy, surface and subsurface soil temperatures, water storage in the three soil layers, and water storage in the canopy), represent most standard land processes. There are 18 surface-cover types and 12 soil types. For each vegetation type, there are about 27 derived parameters, which determine the morphological, physical, and physiological properties of vegetation and soil. The soil surface evaporation is calculated using a demand–supply approach (Dickinson 1984) that depends on the difference between the saturation water vapor specific humidity at soil surface temperature and the specific humidity of the air within the canopy. The vegetation is assumed to be a flat, porous, and uniform layer, where the foliage is assumed to have zero heat capacity. The evapotranspiration from canopy consists of the evaporation from water on wet foliage and the transpiration from dry leaf surfaces.

For this experiment, CCM3/BATS was run at a resolution of 2.8° lat × 2.8° lon. The W and R ensembles both used prescribed July SSTs from 1983. All members of the W ensemble began on 15 June and ran through July; data generated during 15–30 June were ignored. The initial land conditions for the 16 ensemble members were identical, and the initial atmospheric conditions were the atmospheric stages generated on 16 sequential simulation days that span the period from 7 to 23 June from a preliminary simulation using prescribed SSTs from 1983. The 16 ensemble members of the R simulations use that same set of initial conditions.

c. COLA

Version 2.2 of the COLA AGCM is used in this analysis. This model consists of a dynamical core taken from the NCAR CCM3 (Williamson and Olson 1994; Kiehl et al. 1998), and a set of physical parameterizations that include the Mellor and Yamada (1982) turbulence scheme with level 2.0 closure applied throughout the vertical column, the relaxed Arakawa–Schubert scheme for convective precipitation of Moorthi and Suarez (1992), Tiedke (1984) shallow convection, the shortwave radiation parameterization of Lacis and Hansen (1974) as modified by Davies (1982), and the longwave radiation parameterization of Harshvardhan and Corsetti (1984). There is no specific PBL scheme per se.

The land surface scheme is based on the simplified version of the Simple Biosphere (SiB; Sellers et al. 1986) called SSiB (Xue et al. 1991, 1996). This version implements spatially and temporally varying vegetation parameters, and spatially varying soil parameters based on the International Satellite Land Surface Climatology Project (ISLSCP) Initiative I land surface data (Sellers et al. 1996) as described by Dirmeyer and Zeng (1997, 1999). In addition, the full two-stream calculation for surface radiation has been reintroduced (Sellers 1985), and a multilayer temperature diffusion scheme replaces the original force–restore soil temperature scheme (Viterbo and Beljaars 1995).

The grid resolution applied in this experiment was 1.8° lat × 2.8° lon. The 16 sets of initial atmospheric and land states for the W and R ensembles were the 1 July states for the years 1979–95 generated in a preexisting AMIP2 simulation. All members of the W and R ensembles, however, were forced with 1986 SSTs. The member of the W ensemble that provided the time series of states for the R ensemble was the member initialized with the 1986 states. [See Dirmeyer (2001) for details.]

d. HadAM3

HadAM3 is the atmosphere–land component of version 3 of the Hadley Centre Climate Model (Pope et al. 2000). It is a hydrostatic gridpoint model with a standard horizontal resolution of 2.5° lat × 3.75° lon, 19 vertical levels, and a 30-min timestep. Atmospheric dynamics are represented using Eulerian advection on the Arakawa B grid with hybrid vertical coordinates. Convection is modeled using the mass-flux scheme of Gregory and Rowntree (1990), with the addition of convective downdrafts and convective momentum transport (Gregory et al. 1997). The boundary layer scheme employs local mixing on up to five vertical levels, with coefficients dependent on mixing length, local wind shear, and atmospheric stability.

HadAM3 includes the Met Office Surface Exchange Scheme (MOSES) land surface scheme (Cox et al. 1999). The version used here (MOSES I) calculates a single surface energy balance for each grid box using effective surface parameters. The soil state is modeled using four vertical layers, with thicknesses from the surface down of 0.1, 0.25, 0.65, and 2.0 m. Vertical soil moisture movement is parameterized with a finite-difference form of the Richards equation, with account taken for the hydrological and thermodynamic effects of freezing and thawing. Tranpiration from vegetated areas is calculated using a coupled canopy conductance

and photosynthesis scheme (Cox et al. 1998). MOSES I has 10 prognostic variables (four soil temperatures, four soil moistures, snow mass, and intercepted canopy water).

July 1981 SSTs were prescribed in all simulations. The 1 July atmospheric and land conditions simulated for each of the years 1979–94 during a pre-existing AMIP run were used as initial conditions for the 16 members of the W ensemble, and the same sets of atmospheric initial conditions were used for the R ensemble. The R ensemble prescribed the land states generated by the W simulation with the 1 July 1981 initial conditions, resetting the soil temperatures, soil moistures, and snow mass every hour. The canopy water, however, which has a short memory, was allowed to run free in both the R and W ensembles.

REFERENCES

Bonan, G. B., 1998: The land surface climatology of the NCAR Land Surface Model coupled to the NCAR Community Climate Model. *J. Climate,* **11,** 1307–1326.

Boville, B. A., and P. R. Gent, 1998: The NCAR Climate System Model, version one. *J. Climate,* **11,** 1115–1130.

Cox, P. M., C. Huntingford, and R. J. Harding, 1998: A canopy conductance and photosynthesis model for use in a GCM land surface scheme. *J. Hydrol.,* **213,** 79–94.

——, R. A. Betts, C. B. Bunton, R. L. H. Essery, P. R. Rowntree, and J. Smith, 1999: The impact of new land surface physics on the GCM simulation of climate and climate sensitivity. *Climate Dyn.,* **15,** 183–203.

Davies, R., 1982: Documentation of the solar radiation parameterization in the GLAS Climate Model. NASA Tech. Memo 83961, Goddard Space Flight Center, Greenbelt, MD, 57 pp.

Delworth, T. L., and S. Manabe, 1989: The influence of soil wetness on near-surface atmospheric variability. *J. Climate,* **2,** 1447–1462.

Dickinson, R. E., 1984: Modelling evapotranspiration for three dimensional global climate models. *Climate Processes and Climate Sensitivity, Geophys. Monogr.,* No. 29, Amer. Geophys. Union, 58–72.

——, A. Henderson-Sellers, and P. J. Kennedy, 1993: Biosphere–Atmosphere Transfer Scheme (BATS) version 1e as coupled to the NCAR Community Climate Model. NCAR Tech. Note NCAR/TN-387+STR, National Center for Atmospheric Research, Boulder, CO, 72 pp.

Dirmeyer, P. A., 1994: Vegetation stress as a feedback mechanism in midlatitude drought. *J. Climate,* **7,** 1463–1483.

——, 2001: An evaluation of the strength of land–atmosphere coupling. *J. Hydrometeor.,* **2,** 329–344.

——, and F. J. Zeng, 1997: A two-dimensional implementation of the Simple Biosphere (SiB) model. COLA Rep. 48, Center for Ocean–Land–Atmosphere Studies, Calverton, MD, 30 pp.

——, and ——, 1999: An update to the distribution and treatment of vegetation and soil properties in SSiB. COLA Tech. Rep. 78, 25 pp. [Available from the Center for Ocean–Land–Atmosphere Studies, 4041 Powder Mill Road, Suite 302, Calverton, MD 20705.]

Douville, H., F. Chauvin, and H. Broqua, 2001: Influence of soil moisture on the Asian and African monsoons. Part I: Mean monsoon and daily precipitation. *J. Climate,* **14,** 2381–2403.

Findell, K. L., and E. A. B. Eltahir, 1997: An analysis of the soil moisture–rainfall feedback, based on direct observations from Illinois. *Water Resour. Res.,* **33,** 725–735.

Gates, W. L., 1992: AMIP: The atmospheric model intercomparison project. *Bull. Amer. Meteor. Soc.,* **73,** 1962–1970.

Gedney, N., P. M. Cox, H. Douville, J. Polcher, and P. J. Valdes, 2000: Characterizing GCM land-surface schemes to understand their responses to climate change. *J. Climate,* **13,** 3066–3079.

Gregory, D., and P. R. Rowntree, 1990: A mass-flux convection scheme with representation of cloud ensemble characteristics and stability dependent closure. *Mon. Wea. Rev.,* **118,** 1483–1506.

——, R. Kershaw, and P. M. Inness, 1997: Parametrization of momentum transport by convection. II: Tests in single column and general circulation models. *Quart. J. Roy. Meteor. Soc.,* **123,** 1153–1183.

Hack, J. J., 1994: Parameterization of moist convection in the NCAR Community Climate Model (CCM2). *J. Geophys. Res.,* **99,** 5551–5568.

Hahmann, A. N., and R. E. Dickinson, 2001: A fine-mesh land approach for general circulation models and its impact on regional climate. *J. Climate,* **14,** 1634–1646.

Harshvardhan, and T. G. Corsetti, 1984: Longwave radiation parameterization for the UCLA/GLAS GCM. NASA Tech. Memo 86072, Goddard Space Flight Center, Greenbelt, MD, 65 pp.

Henderson-Sellers, A., and V. Gornitz, 1984: Possible climatic impacts of land cover transformations, with particular emphasis on tropical deforestation. *Climatic Change,* **6,** 231–258.

Holtslag, A. A. M., and B. A. Boville, 1993: Local vesus non-local boundary layer diffusion in a global climate model. *J. Climate,* **6,** 1825–1842.

Kiehl, J. T., J. J. Hack, G. B. Bonan, B. A. Boville, D. L. Williamson, and P. J. Rasch, 1998: The National Center for Atmospheric Research Community Climate Model: CCM. *J. Climate,* **11,** 1131–1149.

Koster, R. D., and M. J. Suarez, 1992: Modeling the land surface boundary in climate models as a composite of independent vegetation stands. *J. Geophys. Res.,* **97,** 2697–2715.

——, and ——, 1996: Energy and water balance calculations in the Mosaic LSM. NASA Tech. Memo. 104606, Vol. 9, 60 pp.

——, ——, and M. Heiser, 2000: Variance and predictability of precipitation at seasonal-to-interannual timescales. *J. Hydrometeor.,* **1,** 26–46.

Lacis, A. A., and J. E. Hansen, 1974: A parameterization for the absorption of solar radiation in the earth's atmosphere. *J. Atmos. Sci.,* **31,** 118–133.

Lau, K.-M., and W. Bua, 1998: Mechanisms of monsoon–Southern Oscillation coupling, insights from GCM experiments. *Climate Dyn.,* **14,** 759–779.

Louis, J., M. Tiedtke, and J. Geleyn, 1982: A short history of the PBL parameterization at ECMWF. *ECMWF Workshop on Planetary Boundary Layer Parameterization,* Reading, United Kingdom, ECMWF, 59–80.

Mellor, G. L., and T. Yamada, 1982: Development of a turbulence closure model for geophysical fluid problems. *Rev. Geophys.,* **20,** 851–875.

Moorthi, S., and M. J. Suarez, 1992: Relaxed Arakawa–Schubert, a parameterization of moist convection for general circulation models. *Mon. Wea. Rev.,* **120,** 978–1002.

Oglesby, R. J., and D. J. Erickson III, 1989: Soil moisture and the persistence of North American drought. *J. Climate,* **2,** 1362–1380.

Pope, V. D., M. L. Gallani, P. R. Rowntree, and R. A. Stratton, 2000: The impact of new physical parametrizations in the Hadley Centre climate model—HadAM3. *Climate Dyn.,* **16,** 123–146.

Rowell, D. P., C. Folland, K. Maskell, and M. N. Ward, 1995: Variability of summer rainfall over tropical north Africa (1906–92): Observations and modeling. *Quart. J. Roy. Meteor. Soc.,* **121,** 669–704.

Schar, C., D. Luthi, and U. Beyerle, 1999: The soil–precipitation feedback: A process study with a regional climate model. *J. Climate,* **12,** 722–741.

Sellers, P. J., 1985: Canopy reflectance, photosynthesis and transpiration. *Int. J. Remote Sens.,* **6,** 1335–1372.

——, Y. Mintz, Y. C. Sud, and A. Dalcher, 1986: A simple biosphere

model (SiB) for use within general circulation models. *J. Atmos. Sci.*, **43,** 505–531.

——, and Coauthors, 1996: The ISLSCP Initiative 1 global datasets: Surface boundary conditions and atmospheric forcings for land-atmosphere studies. *Bull. Amer. Meteor. Soc.*, **77,** 1987–2005.

Shukla, J., and Y. Mintz, 1982: Influence of land-surface evapotranspiration on the earth's climate. *Science*, **215,** 1498–1501.

Suarez, M. J., and L. L. Takacs, 1995: Documentation of the ARIES/GEOS Dynamical Core: Version 2. NASA Tech. Memo. 104606, Vol. 5, 53 pp.

Tiedtke, M., 1984: The effect of penetrative cumulus convection on the large scale flow in a general circulation model. *Beitr. Phys. Atmos.*, **57,** 216–239.

Viterbo, P., and A. C. M. Beljaars, 1995: An improved land surface parameterization scheme in the ECMWF model and its validation. *J. Climate*, **8,** 2716–2748.

Williamson, D. L., and J. G. Olson, 1994: Climate simulations with a semi-Lagrangian version of the NCAR Community Climate Model. *Mon. Wea. Rev.*, **122,** 1594–1610.

Xue, Y., P. J. Sellers, J. L. Kinter, and J. Shukla, 1991: A simplified biosphere model for global climate studies. *J. Climate*, **4,** 345–364.

——, F. J. Zeng, and C. A. Schlosser, 1996: SSiB and its sensitivity to soil properties—A case study using HAPEX–Mobilhy data. *Global Planet. Change*, **13,** 183–194.

Zhang, G. J., and N. A. Mcfarlane, 1995: Sensitivity of climate simulations to the parameterization of cumulus convection in the Canadian Climate Center General-Circulation Model. *Atmos.–Ocean*, **33,** 407–446.